Available online at www.sciencedirect.com
SCIENCE DIRECT®
International Journal of Thermal Sciences 44 (2005) 1013–1023
International Journal of Thermal Sciences
www.elsevier.com/locate/ijts

Adaptive solutions of SP_N-approximations to radiative heat transfer in glass ☆

Axel Klar, Jens Lang *, Mohammed Seaïd

Department of Mathematics, Darmstadt University of Technology, 64289 Darmstadt, Germany

Received 4 August 2004; received in revised form 30 January 2005; accepted 7 April 2005

Available online 23 May 2005

Abstract

This paper presents numerical models of radiative heat transfer in glass manufacturing that can be performed on normal workstations, yet are sufficiently accurate for many practical applications. Since many of the glass production processes are so complex that a complete simulation is still unthinkable at present, there is a great interest for such models in order to optimise final glass products. We use simplified approximations of spherical harmonics to obtain approximate solutions of high accuracy in optically thick regimes. The arising systems of partial differential-algebraic equations of mixed parabolic–elliptic type are numerically solved by a self-adaptive discretization method based on an error-controlled finite element method in space and a one-step method of Rosenbrock-type with variable step sizes in time. The method itself judges the quality of the numerical solutions and determines adaptive strategies to keep the discretization error below a user-prescribed tolerance. Multilevel techniques based on reliable and efficient a posteriori error estimators and time embedding are used to improve the spatial discretization by local refinement and to steer the step size selection routine. We present numerical results for a typical step in glass manufacturing, the cooling of a glass cube. Our approximate solutions are validated with solutions to the full radiative transport equation and compared to Rosseland approximations widely used in the engineering practice. The results show that simplified approximations of spherical harmonics are efficient and sufficiently accurate. They are a significant improvement of the classical diffusion models.

Keywords: Radiative heat transfer; Simplified spherical harmonics; Adaptive finite elements; Rosenbrock methods; Glass cooling

1. Introduction

Radiative heat transfer plays an important role in glass manufacturing. Because of the high temperature at which glass is processed, radiation has to be taken into account to accurately compute the temperature distribution in the glass. The temperature has large influence on the precise chemical composition, the viscosity and the internal stresses affecting the quality of the resulting products or devices. Cracks and other defects may cause a high failure rate of finished end-products. Due to the growing success of the polymer industry in many areas, the glass industry is in great need for efficient simulation tools in order to optimise glass production processes.

Thermal radiation has to be modelled by equations that involve the direction- and frequency-dependent thermal radiation field due to the energy transport by photons. The model we consider consists of a heat equation for the temperature $T(\mathbf{x}, t)$ and a transport equation with isotropic scattering for the intensity $I(\mathbf{x}, t, \nu, \mathbf{s})$:

$$\rho_m c_m \partial_t T - \nabla \cdot (k_c \nabla T) = -\int_{\nu_0}^{\infty} \int_{S^2} \kappa \big(B_m(T, \nu) - I\big)\, \mathrm{d}\mathbf{s}\, \mathrm{d}\nu \tag{1}$$

$$\forall \nu > \nu_0\colon\ \mathbf{s} \cdot \nabla I + (\sigma + \kappa) I = \frac{\sigma}{4\pi} \int_{S^2} I\, \mathrm{d}\mathbf{s} + \kappa B_m(T, \nu) \tag{2}$$

☆ A preliminary version of this paper was presented at CHT-04: An ICHMT International Symposium on Advances in Computational Heat Transfer, April 2004, G. de Vahl Davis and E. Leonardi (Eds.), CD-ROM Proceedings, ISBN 1-5670-174-2, Begell House, New York, 2004

* Corresponding author.
E-mail address: lang@mathematik.tu-darmstadt.de (J. Lang).

1290-0729/$ – see front matter
doi:10.1016/j.ijthermalsci.2005.04.001

Nomenclature

a_1, a_2	constants
B_m	Planck function
b_i	coefficient of ROM
c	speed of light in the medium
c_0	speed of light in vacuum
c_m	specific heat capacity
c_{ij}	coefficients of ROM
d	space dimension
d_1, d_2	constants
$\mathbf{e}$	local spatial error
h_c	convective heat transfer coefficient
h_P	Planck constant
I	Intensity
$\mathbf{J}$	Jacobian
k_B	Boltzmann constant
k_c	thermal conductivity
k_r	thermal conductivity caused by radiation
L_n	linear differential operator
$\mathbf{n}$	outward normal vector
n_m	refractive index
n_a	refractive index of air
n_g	refractive index of glass
Q_ω	finite element space
ROM	Rosenbrock method
r_1, r_2	constants
$\mathbf{s}$	direction on S^2
$\mathbf{s}'$	specular reflection of $\mathbf{s}$
S^2	unit sphere
S_h^1	finite element space
SP_N	simplified P_N
t	time
t_e	final integration time
T	temperature
T_b, T_0	ambient and initial temperature
$\mathbf{v}, \mathbf{V}$	vectors
$\mathbf{x}$	Cartesian spatial coordinates

Greek symbols

α	mean hemispheric surface emissivity
α_1, α_2	constants
α_{ij}	coefficient of ROM
β_1, β_2	constants
γ	stability parameter of ROM
γ_1, γ_2	constants
ϵ	dimensionless parameter
ε_n	estimator of the local temporal error
η, η_k	local discretization errors
κ, κ_i	absorption
μ_1, μ_2	constants
ν	frequency
ν_0	upper bound of opaque spectral region
ϕ, ϕ_i	integrated intensity
ψ_1, ψ_2	functions related to ϕ
ρ	reflectivity
ρ_m	density
σ, σ_i	scattering
ω	union of finite elements
ω_i	weights
Ω	convex space domain
$\partial\Omega$	boundary of Ω
τ_i, τ_n	time steps
Θ_g, Θ_a	refraction angles in glass and air
$\boldsymbol{\xi}$	finite element ansatz function

Subscripts

m	medium, or dimension of vectors
n	time level
i	stage level of ROM, or frequency band
ref	reference quantities
h	mesh width

Superscript

n	time level

where $(\mathbf{x}, t, \nu, \mathbf{s}) \in \Omega \times [0, t_e) \times [0, \infty) \times S^2$ for the spatial, time, frequency, and directional variables. Here, Ω is a given two- or three-dimensional convex space domain with boundary $\partial\Omega$ and S^2 is the unit sphere. The physical parameters are denoted by ρ_m for the density, c_m for the specific heat capacity, k_c for the thermal conductivity, κ for the absorption, and σ for the scattering.

The Planck function or monochromatic black-body intensity is defined as

$$B_m(T, \nu) = \frac{n_m^2}{c_0^2} \frac{2h_P \nu^3}{e^{h_P \nu/(k_B T)} - 1} \tag{3}$$

with $h_P := 6.62608 \times 10^{-34}$ Js for the Planck constant and $k_B := 1.38066 \times 10^{-23}$ J·K^{-1} for the Boltzmann constant. The refractive index n_m is the ratio of the speed of light in vacuum and within the medium

$$n_m := \frac{c_0}{c} \tag{4}$$

We introduce $B_{\text{air}}(T, \nu)$ and $B_{\text{glass}}(T, \nu)$ setting $n_m := n_a = 1$ for air and $n_m := n_g = 1.46$ for glass in (3). The specific frequency ν_0 defines the opaque interval $[0, \nu_0]$ of the spectrum. On the boundary $\partial\Omega$, the temperature satisfies

$$k_c \mathbf{n} \cdot \nabla T = h_c(T_b - T) + \alpha\pi \int_0^{\nu_0} \big(B_{\text{air}}(T_b, \nu) - B_{\text{air}}(T, \nu)\big)\, \mathrm{d}\nu \tag{5}$$

where we assume the outside medium to be air. The heat flux through the boundary is determined by free convection

of the surrounding air and diffusive surface radiation [1]. Here, $\mathbf{n} = \mathbf{n}(\mathbf{x})$ denotes the outward normal in $\mathbf{x} \in \partial\Omega$, h_c is the convective heat transfer coefficient, T_b the ambient temperature, and α is the mean hemispheric surface emissivity in the opaque spectral region. In our computation, we use $\alpha = 0.914$. The temperature at the beginning is prescribed by

$$T(\mathbf{x}, 0) = T_0(\mathbf{x}), \quad \mathbf{x} \in \Omega \tag{6}$$

Since Eq. (2) for the intensity is a first order differential equation, we need to specify incident radiation on $\Gamma^- := \{(\mathbf{x}, \mathbf{s}) \in \partial\Omega \times S^2 : \mathbf{n}(\mathbf{x}) \cdot \mathbf{s} < 0\}$. It is described by semi-transparent boundary conditions

$$\begin{aligned} &I(\mathbf{x}, t, \nu, \mathbf{s}) \\ &\quad = \rho(\mathbf{n} \cdot \mathbf{s}) I(\mathbf{x}, t, \nu, \mathbf{s}') \\ &\qquad + \big(1 - \rho(\mathbf{n} \cdot \mathbf{s})\big) B_{\text{glass}}(T_b, \nu), \quad (\mathbf{x}, \mathbf{s}) \in \Gamma^- \end{aligned} \tag{7}$$

where $\mathbf{s}' = \mathbf{s} - 2(\mathbf{n} \cdot \mathbf{s})\mathbf{n}$ is the specular reflection of $\mathbf{s}$ on $\partial\Omega$. The reflectivity $\rho \in [0, 1]$ determines the amount of radiative energy that is reflected and can be found using Fresnel's reflection equation

$$\rho(\mathbf{n} \cdot \mathbf{s}) = \frac{1}{2}\left[\frac{\tan^2(\Theta_g - \Theta_a)}{\tan^2(\Theta_g + \Theta_a)} + \frac{\sin^2(\Theta_g - \Theta_a)}{\sin^2(\Theta_g + \Theta_a)}\right] \tag{8}$$

where the refraction angles Θ_g and Θ_a in glass and air are given by $\cos\Theta_g = |\mathbf{n} \cdot \mathbf{s}|$ and by Snell's law

$$n_g \sin\Theta_g = n_a \sin\Theta_a \tag{9}$$

Since $n_a < n_g$, a critical angle $\Theta_g^* = \arcsin(n_a/n_g)$ exists, such that the refraction direction is parallel to the surface. For angles greater than Θ_g^*, all radiative energy is reflected, i.e., $\rho = 1$. We assume that the reflectivity does not depend on frequency. Since not much data is available about the reflective interaction between glass and opaque boundaries, we do not distinguish between opaque and nonopaque part of the spectrum at the boundary. Note that many physical assumptions have to be taken into account to derive well-posed models for radiative heat transfer. For more details on these assumptions, we refer to [2–4].

Eqs. (1)–(7) form our radiative heat transfer model. The intensity I is not only a function of the spatial coordinate and the time, but also depends on two directional coordinates and the frequency. Even with the permanently growing computer power, this high dimension of the phase space makes the numerical solution of the radiative heat transfer equations (RHTE) difficult and expensive, especially in real-life three-dimensional applications. Nowadays there is an increasing activity to derive numerical models for the RHTE that are computationally less time consuming, yet sufficiently accurate. Among others, we find the ray-tracing method [5–7] which solves (2) exactly along rays for a given temperature distribution, the discrete ordinate method, where only a finite number of directions is considered [8,9], the method of spherical harmonics (P_N-approximations), and various diffusion approximations. The Rosseland approximation [10] is the simplest diffusion approximation and therefore the fastest method for radiative heat transfer. Although its assumptions are often invalid, it is widely used in existing simulations of glass production. Improved diffusion approximations are proposed in [11].

In this paper, we consider simplified P_N-approximations (SP_N) applied to optically thick situations. SP_N-approximations were firstly proposed by Gelbard [12] and later on theoretically founded by Larsen et al. [13]. In [14] the SP_N-equations have been tested fairly extensively for various radiation transfer problems in glass and have proven to be an efficient way to improve the classical diffusion approximations. They yield accurate approximations to the RHTE even when the regime becomes less diffusive.

The SP_N-approximations result in a system of partial differential algebraic equations (PDAE) of mixed parabolic–elliptic type. This PDAE-system can then be attacked by a fully adaptive discretization method which is able to judge the quality of the numerical approximation and to determine an adaptive strategy to improve the accuracy up to a user-prescribed tolerance where needed. In this work, we use a combination of an error-controlled finite element method based on local grid refinement and an efficient variable step size one-step method of linearly implicit type [15,16]. Multilevel techniques based on reliable and efficient a posteriori error estimators and time embedding are used to improve the spatial discretization in each time step and to steer the step size selection routine. These features free us from designing special fixed meshes and step sizes where a priori knowledge about the regions of main solution activities is required and from tuning various solution parameters. The method saves a vast amount of computer power and can be performed on normal workstations.

The paper is organized as follows. First, we formulate simplified SP_N-approximations in dimensionless form and state models that are based on frequency bands with piecewise constant absorption and scattering rates. Then we describe our adaptive time and space discretizations. Finally, numerical two- and three-dimensional simulations are presented and a conclusion is given.

2. Simplified P_N-approximations

We rewrite the RHTE in a dimensionless form, introducing the following non-dimensional variables

$$t^* = \frac{t}{t_{\text{ref}}}, \qquad x^* = \frac{x}{x_{\text{ref}}}, \qquad T^* = \frac{T}{T_{\text{ref}}}, \qquad I^* = \frac{I}{I_{\text{ref}}}$$

$$\sigma^* = \frac{\sigma}{\sigma_{\text{ref}} + \kappa_{\text{ref}}}, \qquad \kappa^* = \frac{\kappa}{\sigma_{\text{ref}} + \kappa_{\text{ref}}}$$

$$k_c^* = \frac{k_c}{k_{c,\text{ref}}}, \qquad h_c^* = \frac{h_c}{h_{c,\text{ref}}}$$

where the subscript ref corresponds to reference quantities. We impose the relations

$$t_{\text{ref}} = c_m \rho_m (\sigma_{\text{ref}} + \kappa_{\text{ref}}) x_{\text{ref}}^2 \frac{T_{\text{ref}}}{I_{\text{ref}}}$$

$$k_{c,\text{ref}} = \frac{I_{\text{ref}}}{(\sigma_{\text{ref}} + \kappa_{\text{ref}}) T_{\text{ref}}}, \qquad h_{c,\text{ref}} = \frac{I_{\text{ref}}}{T_{\text{ref}}}$$

and introduce the dimensionless parameter

$$\epsilon := \frac{1}{(\sigma_{\text{ref}} + \kappa_{\text{ref}}) x_{\text{ref}}}$$

which satisfies $0 < \epsilon \ll 1$ in the optically thick, diffusive regime. The system of scaled equations reads

$$\epsilon^2 \partial_t T - \epsilon^2 \nabla \cdot (k_c \nabla T) = -\int_{\nu_0}^{\infty} \int_{S^2} \kappa \big(B^*_{\text{glass}}(T, \nu) - I \big) \, \mathrm{d}\mathbf{s} \, \mathrm{d}\nu \tag{10}$$

$$\epsilon \mathbf{s} \cdot \nabla I + (\sigma + \kappa) I = \frac{\sigma}{4\pi} \int_{S^2} I \, \mathrm{d}\mathbf{s} + \kappa B^*_{\text{glass}}(T, \nu) \quad \forall \nu > \nu_0 \tag{11}$$

$$\epsilon k_c \mathbf{n} \cdot \nabla T = h_c (T_b - T) + \alpha\pi \int_0^{\nu_0} \big(B^*_{\text{air}}(T_b, \nu) - B^*_{\text{air}}(T, \nu) \big) \, \mathrm{d}\nu \tag{12}$$

$$I(\mathbf{x}, t, \nu, \mathbf{s}) = \rho(\mathbf{n} \cdot \mathbf{s}) I(\mathbf{x}, t, \nu, \mathbf{s}') + \big(1 - \rho(\mathbf{n} \cdot \mathbf{s})\big) B^*_{\text{glass}}(T_b, \nu) \tag{13}$$

$$T(\mathbf{x}, 0) = T_0(\mathbf{x}) \tag{14}$$

where we have dropped the asterisk of the dimensionless variables for ease of notation. The expression $B^*_m(T, \nu)$ is defined by

$$B^*_m(T, \nu) := \frac{B_m(T \cdot T_{\text{ref}}, \nu)}{I_{\text{ref}}}$$

If scattering is large and absorption weak, an asymptotic (for $\epsilon \ll 1$) expansion of (10)–(14) yields the *equilibrium diffusion* or *Rosseland approximation*

$$\partial_t T - \nabla \cdot \big((k_c + k_r(T)) \nabla T \big) = 0$$

$$k_r(T) = \frac{4\pi}{3} \int_{\nu_0}^{\infty} \frac{1}{\sigma + \kappa} \partial_T B^*_{\text{glass}}(T, \nu) \, \mathrm{d}\nu \tag{15}$$

$$\epsilon k_c \mathbf{n} \cdot \nabla T = h_c (T_b - T) + \alpha\pi \int_0^{\nu_0} \big(B^*_{\text{air}}(T_b, \nu) - B^*_{\text{air}}(T, \nu) \big) \, \mathrm{d}\nu \tag{16}$$

$$T(\mathbf{x}, 0) = T_0(\mathbf{x}) \tag{17}$$

Unfortunately, this relatively simple diffusion approximation gives unsatisfactory results for boundary layers which are already present in glass cooling processes due to large temperature gradients at the boundary.

Recently, higher-order asymptotic corrections in ϵ to the Rosseland approximation known as simplified P_N-approximations (SP_N) have been derived and numerically tested [4,14]. These models are able to describe boundary layers more accurate while keeping the computational complexity on an acceptable level.

The SP_1-approximation for the RHTE reads

$$\partial_t T - \nabla \cdot (k_c \nabla T) = \int_{\nu_0}^{\infty} \nabla \cdot \left(\frac{1}{3(\sigma + \kappa)} \nabla \phi \right) \mathrm{d}\nu \tag{18}$$

$$-\epsilon^2 \nabla \cdot \left(\frac{1}{3(\sigma + \kappa)} \nabla \phi \right) + \kappa \phi = 4\pi \kappa B^*_{\text{glass}}(T, \nu) \quad \forall \nu > \nu_0 \tag{19}$$

with the integrated intensity $\phi = \int_{S^2} I \, \mathrm{d}\mathbf{s}$ and the boundary and initial conditions

$$k_c \mathbf{n} \cdot \nabla T = \frac{h_c}{\epsilon} (T_b - T) + \frac{\alpha\pi}{\epsilon} \int_0^{\nu_0} \big(B^*_{\text{air}}(T_b, \nu) - B^*_{\text{air}}(T, \nu) \big) \, \mathrm{d}\nu \tag{20}$$

$$\frac{\epsilon}{3(\sigma + \kappa)} \mathbf{n} \cdot \nabla \phi = \frac{1 - 2r_1}{2 + 6r_2} \big(4\pi B^*_{\text{glass}}(T_b, \nu) - \phi \big) \tag{21}$$

$$T(\mathbf{x}, 0) = T_0(\mathbf{x}) \tag{22}$$

where $r_1 = 0.2855742$ and $r_2 = 0.1452082$ for the glass–air boundary interface (see [14] for a detailed analysis). From (19), we get $\phi = 4\pi B^*_{\text{glass}}(T, \nu) + \mathrm{O}(\epsilon^2)$. Using this relation in (18), we recover the Rosseland approximation (15).

The SP_3-approximation is given by

$$\partial_t T - \nabla \cdot (k_c \nabla T) = \int_{\nu_0}^{\infty} \nabla \cdot \left(\frac{1}{\sigma + \kappa} \nabla (a_1 \psi_1 + a_2 \psi_2) \right) \mathrm{d}\nu \tag{23}$$

$$-\epsilon^2 \nabla \cdot \left(\frac{\mu_1^2}{\sigma + \kappa} \nabla \psi_1 \right) + \kappa \psi_1 = 4\pi \kappa B^*_{\text{glass}}(T, \nu) \quad \forall \nu > \nu_0 \tag{24}$$

$$-\epsilon^2 \nabla \cdot \left(\frac{\mu_2^2}{\sigma + \kappa} \nabla \psi_2 \right) + \kappa \psi_2 = 4\pi \kappa B^*_{\text{glass}}(T, \nu) \quad \forall \nu > \nu_0 \tag{25}$$

with the boundary and initial conditions

$$k_c \mathbf{n} \cdot \nabla T = \frac{h_c}{\epsilon} (T_b - T) + \frac{\alpha\pi}{\epsilon} \int_0^{\nu_0} \big(B^*_{\text{air}}(T_b, \nu) - B^*_{\text{air}}(T, \nu) \big) \, \mathrm{d}\nu \tag{26}$$

$$\frac{\epsilon}{\sigma + \kappa} \mathbf{n} \cdot \nabla \psi_1 = \gamma_1 \pi B^*_{\text{glass}}(T_b, \nu) - \alpha_1 \psi_1 - \beta_2 \psi_2 \tag{27}$$

$$\frac{\epsilon}{\sigma + \kappa} \mathbf{n} \cdot \nabla \psi_2 = \gamma_2 \pi B^*_{\text{glass}}(T_b, \nu) - \beta_1 \psi_1 - \alpha_2 \psi_2 \tag{28}$$

$$T(\mathbf{x}, 0) = T_0(\mathbf{x}) \tag{29}$$

The constants appearing in the equations are

$$a_n = \frac{1}{30}\left(5 + (-1)^n\sqrt{\frac{5}{6}}\right)$$

$$\mu_n^2 = \frac{1}{7}\left(3 + 2(-1)^n\sqrt{\frac{6}{5}}\right), \quad n = 1, 2$$

The integrated intensity ϕ can be recovered from a linear combination of ψ_1 and ψ_2

$$\phi = \frac{d_2\psi_1 - d_1\psi_2}{d_2 - d_1}$$

$$\text{with } d_n = \frac{5}{7}\left(1 + 3(-1)^n\sqrt{\frac{6}{5}}\right), \quad n = 1, 2 \tag{30}$$

For the boundary conditions, we find for the glass–air interface [14]

$$\alpha_1 = 0.084075389781548382$$

$$\alpha_2 = 0.872433935441263020$$

$$\beta_1 = -0.08086509944859642$$

$$\beta_2 = -0.29284032175563224$$

$$\gamma_1 = -0.83505972789633554$$

$$\gamma_2 = 3.1662753439706663$$

The SP_1- and SP_3-equations are independent of the directional variable **s**. They are $O(\epsilon^2)$- and $O(\epsilon^6)$-approximations to the full RHTE. Numerical simulations presented in [4, 14] and in the present paper show that these equations give accurate results in the optically thick and diffusive regime ($\epsilon \ll 1$), but also when the problem becomes less diffusive. The boundary conditions described above are obtained from variational principles and, in special cases, reduce to Marshak boundary conditions which are well-known in neutron transport.

3. Frequency bands model

The SP_N-approximations still contain the frequency variable ν. In simulations of glass cooling, frequency is usually split up into frequency bands $[\nu_{i-1}, \nu_i]$, $i = 1, 2, \ldots, N$, with $\nu_N = \infty$ and piecewise constant absorption and scattering rates

$$\kappa(\nu) = \kappa_i, \qquad \sigma(\nu) = \sigma_i$$
$$\text{for } \nu \in [\nu_{i-1}, \nu_i],\ i = 1, \ldots, N \tag{31}$$

Defining the new variables

$$\phi_i := \int_{\nu_{i-1}}^{\nu_i} \phi \,\mathrm{d}\nu, \qquad \psi_{n,i} := \int_{\nu_{i-1}}^{\nu_i} \psi_n \,\mathrm{d}\nu, \quad n = 1, 2 \tag{32}$$

and integrating Eqs. (19), (21), (24), (25), (27), and (28) over $[\nu_{i-1}, \nu_i]$, we finally end up with a system of $N + 1$ and $2N + 1$ partial differential–algebraic equations (PDAEs) for the SP_1- and SP_3-approximation, respectively.

SP_1-approximation.

$$\partial_t T - \nabla\cdot(k_c\nabla T) = \sum_{i=1}^{N} \nabla\cdot\left(\frac{1}{3(\sigma_i+\kappa_i)}\nabla\phi_i\right) \tag{33}$$

$$-\epsilon^2\nabla\cdot\left(\frac{1}{3(\sigma_i+\kappa_i)}\nabla\phi_i\right) + \kappa_i\phi_i = 4\pi\kappa_i\int_{\nu_{i-1}}^{\nu_i} B^*_{\text{glass}}(T,\nu)\,\mathrm{d}\nu, \quad i = 1, \ldots, N \tag{34}$$

$$k_c\mathbf{n}\cdot\nabla T + \sum_{i=1}^{N}\frac{1}{3(\sigma_i+\kappa_i)}\mathbf{n}\cdot\nabla\phi_i = \frac{h_c}{\epsilon}(T_b - T) + \frac{\alpha\pi}{\epsilon}\int_0^{\nu_0}\left(B^*_{\text{air}}(T_b,\nu) - B^*_{\text{air}}(T,\nu)\right)\mathrm{d}\nu + \frac{1-2r_1}{\epsilon(2+6r_2)}\sum_{i=1}^{N}\left(4\pi\int_{\nu_{i-1}}^{\nu_i} B^*_{\text{glass}}(T_b,\nu)\,\mathrm{d}\nu - \phi_i\right) \tag{35}$$

$$\frac{\epsilon^2}{3(\sigma_i+\kappa_i)}\mathbf{n}\cdot\nabla\phi_i = \frac{\epsilon(1-2r_1)}{2+6r_2}\left(4\pi\int_{\nu_{i-1}}^{\nu_i} B^*_{\text{glass}}(T_b,\nu)\,\mathrm{d}\nu - \phi_i\right), \quad i = 1, \ldots, N \tag{36}$$

$$T(\mathbf{x}, 0) = T_0(\mathbf{x}) \tag{37}$$

SP_3-approximation.

$$\partial_t T - \nabla\cdot(k_c\nabla T) = \sum_{i=1}^{N}\nabla\cdot\left(\frac{1}{\sigma_i+\kappa_i}\nabla(a_1\psi_{1,i} + a_2\psi_{2,i})\right) \tag{38}$$

$$-\epsilon^2\nabla\cdot\left(\frac{\mu_1^2}{\sigma_i+\kappa_i}\nabla\psi_{1,i}\right) + \kappa_i\psi_{1,i} = 4\pi\kappa_i\int_{\nu_{i-1}}^{\nu_i} B^*_{\text{glass}}(T,\nu)\,\mathrm{d}\nu, \quad i = 1, \ldots, N \tag{39}$$

$$-\epsilon^2\nabla\cdot\left(\frac{\mu_2^2}{\sigma_i+\kappa_i}\nabla\psi_{2,i}\right) + \kappa_i\psi_{2,i} = 4\pi\kappa_i\int_{\nu_{i-1}}^{\nu_i} B^*_{\text{glass}}(T,\nu)\,\mathrm{d}\nu, \quad i = 1, \ldots, N \tag{40}$$

$$k_c\mathbf{n}\cdot\nabla T + \sum_{i=1}^{N}\frac{1}{\sigma_i+\kappa_i}\mathbf{n}\cdot(a_1\nabla\psi_{1,i} + a_2\nabla\psi_{2,i}) = \frac{h_c}{\epsilon}(T_b - T) + \frac{\alpha\pi}{\epsilon}\int_0^{\nu_0}\left(B^*_{\text{air}}(T_b,\nu) - B^*_{\text{air}}(T,\nu)\right)\mathrm{d}\nu$$

$$+\frac{\pi}{\epsilon}(a_1\gamma_1+a_2\gamma_2)\int_{\nu_0}^{\infty} B^*_{\text{glass}}(T_b,\nu)\,\mathrm{d}\nu - \frac{1}{\epsilon}\sum_{i=1}^{N}\big((a_1\alpha_1+a_2\beta_1)\psi_{1,i}+(a_1\beta_2+a_2\alpha_2)\psi_{2,i}\big) \tag{41}$$

$$\frac{\epsilon^2\mu_1^2}{\sigma_i+\kappa_i}\mathbf{n}\cdot\nabla\psi_{1,i} = \epsilon\mu_1^2\left(\gamma_1\pi\int_{\nu_{i-1}}^{\nu_i} B^*_{\text{glass}}(T_b,\nu)\,\mathrm{d}\nu-\alpha_1\psi_{1,i}-\beta_2\psi_{2,i}\right) \tag{42}$$

$$\frac{\epsilon^2\mu_2^2}{\sigma_i+\kappa_i}\mathbf{n}\cdot\nabla\psi_{2,i} = \epsilon\mu_2^2\left(\gamma_2\pi\int_{\nu_{i-1}}^{\nu_i} B^*_{\text{glass}}(T_b,\nu)\,\mathrm{d}\nu-\beta_1\psi_{1,i}-\alpha_2\psi_{2,i}\right) \tag{43}$$

$$i=1,\dots,N$$

$$T(\mathbf{x},0)=T_0(\mathbf{x}) \tag{44}$$

The boundary conditions are formulated in such a way that they can be directly used in a variational formulation of the underlying PDAEs.

The SP_N-equations described here give accurate results for many problems in glass manufacturing. Nevertheless a more detailed investigation of the applicability of the approximations in special cases like systems with void regions and nonconvex domains has to be performed. For further discussions we refer to [14] and the literature given there.

4. Adaptive time and space discretizations

Each of the systems described above can be written in an abstract form of a quasilinear initial-value problem

$$H\partial_t\mathbf{v}+\nabla\cdot\mathbf{J}(\mathbf{v})+\mathbf{R}(\mathbf{v})=0 \quad \text{in } \Omega\times[0,t_e) \tag{45}$$

$$\mathbf{v}(t=0)=\mathbf{v}^0 \quad \text{in } \Omega \tag{46}$$

where

$$\mathbf{v}=\begin{cases} T & \text{for the Rosseland approximation}\\ (T,\phi_1,\dots,\phi_N)^{\mathrm{T}} & \text{for the } SP_1\text{-approximation}\\ (T,\psi_{1,1},\psi_{2,1},\dots,\psi_{1,N},\psi_{2,N})^{\mathrm{T}} & \text{for the } SP_3\text{-approximation}\end{cases}$$

is the m-dimensional solution vector with $m=1,N+1,2N+1$, respectively. The $m\times m$-matrix H is diagonal and has one nonzero entry, i.e., $H=\mathrm{diag}(1,0,\dots,0)$. The first component of the source vector $\mathbf{R}(\mathbf{v})$ that corresponds to the temperature vanishes. The flux vector $\mathbf{J}(\mathbf{v})$ is supplemented with the boundary conditions stated above. Initial values for $\phi_i,\psi_{1,i},\psi_{2,i}$, $i=1,\dots,N$, have to be calculated from the linear elliptic equations setting $T=T_0$ in (34), (39) and (40).

The principle difficulties in solving the system (45), (46) numerically are the strong nonlinearities, the differential–algebraic structure, and the presence of differential operators making the problem infinitely stiff. In such a situation, an implicit or semi-implicit discretization method should be applied to integrate in time. We use linearly implicit methods of Rosenbrock type which are constructed by working the exact Jacobian directly into the formula—an idea which was first proposed by Rosenbrock [17]. Applied to (45), (46) a so-called s-stage Rosenbrock method has the recursive form

$$\mathbf{v}_n=\mathbf{v}_{n-1}+\sum_{i=1}^{s} b_i\mathbf{V}_i^n \tag{47}$$

$$\left(\frac{H}{\gamma\tau_n}+A(\mathbf{v}_{n-1})\right)\mathbf{V}_i^n = \sum_{j=1}^{i-1}\frac{c_{ij}}{\tau_n}H\mathbf{V}_j^n-\nabla\cdot\mathbf{J}\left(\mathbf{v}_{n-1}+\sum_{j=1}^{i-1}\alpha_{ij}\mathbf{V}_j^n\right) - \mathbf{R}\left(\mathbf{v}_{n-1}+\sum_{j=1}^{i-1}\alpha_{ij}\mathbf{V}_j^n\right),\quad i=1,\dots,s \tag{48}$$

where $\mathbf{v}_n$ denotes an approximation of $\mathbf{v}(t_n)$ at $t_n=\sum_{i=1,\dots,n}\tau_i$ and A is the Jacobian matrix $\partial(\nabla\cdot\mathbf{J}(\mathbf{v})+\mathbf{R}(\mathbf{v}))/\partial\mathbf{v}$. The coefficients γ, α_{ij}, c_{ij}, and b_i are chosen to obtain good stability properties for stiff equations and a desired order of consistency. In this work, we have used the third-order Rosenbrock solver ROS3P with three stages proposed in [18]. The corresponding coefficients are presented in Table 1. The fundamental idea of linearly implicit methods is that for the calculation of the intermediate values $\mathbf{V}_i^n$, $i=1,\dots,s$, only a sequence of linear systems with one and the same operator have to be solved. An iterative Newton method as known from (fully) implicit time discretizations is no longer required. More details can be found in [19].

The specific structure of the Rosenbrock method (47), (48) allows us to construct an embedded solution of inferior order

$$\mathbf{v}_n^*=\mathbf{v}_{n-1}+\sum_{i=1}^{s} b_i^*\mathbf{V}_i^n \tag{49}$$

replacing the coefficients b_i in (47) by a different set of coefficients b_i^*. The embedded solution of ROS3P has order

Table 1
Set of coefficients for the 3-stage ROS3P method [18]

$\gamma = 7.886751345948129\text{e}{-01}$	
$\alpha_{21} = 1.267949192431123\text{e}{+00}$	$c_{21} = 1.607695154586736\text{e}{+00}$
$\alpha_{31} = 1.267949192431123\text{e}{+00}$	$c_{31} = 3.464101615137755\text{e}{+00}$
$a_{32} = 0.000000000000000\text{e}{+00}$	$c_{32} = 1.732050807568877\text{e}{+00}$
$b_1 = 2.000000000000000\text{e}{+00}$	$b_1^* = 2.113248654051871\text{e}{+00}$
$b_2 = 5.773502691896258\text{e}{-01}$	$b_2^* = 1.000000000000000\text{e}{+00}$
$b_3 = 4.226497308103742\text{e}{-01}$	$b_3^* = 4.226497308103742\text{e}{-01}$

two. The difference between the two solutions is then used to estimate the local temporal error by

$$\varepsilon_n := \|\mathbf{v}_n - \mathbf{v}_n^*\|_\Omega \tag{50}$$

In practical applications it is often decisive to choose the norm carefully in order to reflect accurately the scale of the problem. We employ here the weighted root mean square norm

$$\|\mathbf{v}_n - \mathbf{v}_n^*\|_\Omega := \left(\frac{1}{m}\sum_{i=1}^{m}\frac{\|v_{n,i} - v_{n,i}^*\|_{L_2(\Omega)}^2}{w_i^2}\right)^{1/2} \tag{51}$$

with weights

$$w_i = \mathrm{ATOL}_i + \mathrm{RTOL}_i\,\|U_{n,i}\|_{L_2(\Omega)} \tag{52}$$

Here, $\mathbf{U}_n = (U_{n,1}, \ldots, U_{n,m})$ should be a good approximation to the actual solution at $t = t_n$. The values ATOL_i and RTOL_i have to be selected carefully to furnish meaningful input for the error control.

Given a tolerance TOL_t for the time discretization, a standard strategy is to choose the step size of the time step according to

$$\tau_{n+1} = \frac{\tau_n}{\tau_{n-1}}\left(\frac{\mathrm{TOL}_t\,\varepsilon_{n-1}}{\varepsilon_n^2}\right)^{1/3}\tau_n \tag{53}$$

The proposed step τ_{n+1} is then executed. If the new error ε_{n+1} computed from (50) is less than TOL_t the solution $\mathbf{v}_{n+1}$ is accepted. Otherwise, the solution is rejected and the time step is repeated with a reduced value of τ_{n+1}. Formula (53) is related to a discrete PI-controller first established by Gustafsson et al. [20].

The linear problems (47), (48) have to be solved for the intermediate values $\mathbf{V}_i^n$, $i = 1, \ldots, s$. To get the right boundary conditions, the Rosenbrock scheme (47), (48) must be also applied to the nonlinear algebraic equations describing the solution on the boundary. The arising elliptic boundary value problems are solved by a multilevel finite element method. The main idea of the multilevel technique consists of replacing the solution space by a sequence of discrete spaces with successively increasing dimensions to improve the approximation property. It has proven to be a useful tool for drastically reducing the size of the arising linear systems and to achieve high and controlled accuracy of the spatial discretization [15,21,22].

The starting point of the finite element method is the weak formulation of (47), (48). Let Ω_h be a permissible triangulation of $\Omega \subset \mathbb{R}^d$ into finite elements and let S_h^1 consists of all continuous vector functions the components of which are polynomials of first order on each element. We use triangles for $d = 2$ and tetrahedra for $d = 3$. The finite element approximations $\mathbf{V}_{i,h}^n \in S_h^1$, $i = 1, \ldots, s$, have then to satisfy the equations

$$\left(L_n\mathbf{V}_{i,h}^n, \boldsymbol{\xi}\right) = \left(\mathbf{r}_i^n, \boldsymbol{\xi}\right) \quad \text{for all } \boldsymbol{\xi} \in S_h^1 \tag{54}$$

where L_n is the weak representation of the differential operator at the left-hand side in (48) and $\mathbf{r}_i^n$ stands for the entire right-hand side of the ith equation in (48). Since the operator L_n is independent of i its calculation is required only once within each time step.

After computing the approximate intermediate values, a posteriori error estimators can be utilized to give specific assessment of the error distribution. The spatial errors $\mathbf{e}_i^n = \mathbf{V}_i^n - \mathbf{V}_{i,h}^n$ are estimated by solving local Dirichlet problems on small subdomains. Let ω be the union of two elements having one common edge and let Q_ω consists of all continuous vector functions the components of which are polynomials of second order on each element belonging to ω. The local errors $\mathbf{e}_i^n$ are then approximated by $\mathbf{e}_{i,h}^n \in Q_\omega$ satisfying

$$\begin{aligned}\left(L_n\mathbf{e}_{i,h}^n, \boldsymbol{\xi}\right) = \big(&\mathbf{r}_i^n\left(\mathbf{e}_{1,h}^n + \mathbf{V}_{1,h}^n, \ldots, \mathbf{e}_{i-1,h}^n + \mathbf{V}_{i-1,h}^n\right)\\ &- L_n\mathbf{V}_{i,h}^n, \boldsymbol{\xi}\big)\end{aligned} \tag{55}$$

$$\mathbf{e}_{i,h}^n = 0 \quad \text{on } \partial\omega \quad i = 1, \ldots, s, \text{ for all } \boldsymbol{\xi} \in Q_\omega \tag{56}$$

Once the approximate local spatial errors have been computed, we can estimate the local error of the discrete Rosenbrock solution $\mathbf{v}_{n,h} = \mathbf{v}_{n-1,h} + \sum_{i=1,\ldots,s} b_i\mathbf{V}_{i,h}^n$ by

$$\eta := \left\| P\mathbf{v}_{n-1,h} + \sum_{i=1}^{s} b_i\mathbf{e}_{i,h}^n \right\|_\omega \tag{57}$$

Here, $P\mathbf{v}_{n-1,h}$ stands for the projection error resulting from representing the old solution $\mathbf{v}_{n-1,h}$ on the new mesh designed for $\mathbf{v}_{n,h}$. The error estimator η is an asymptotically upper bound for the norm of the local error. For more details, we refer the interested reader to [15]. The estimation procedure is applied all over the computational domain. In order to produce a nearly optimal finite element mesh, subdomains ω_k having an error η_k larger than the mean square value of all errors are refined. In the two-dimensional case, elements marked for refinement are divided into four congruent triangles (*red* refinement). After that triangles with two or three refined edges are compulsory refined *red*; triangles with only one refined edge are subdivided into two triangles (*green* closure). *Green* elements are removed before the next refinement to avoid bad geometric properties of the triangulation. This refinement strategy has been successfully extended to three space dimensions and is nowadays standard (see, e.g., [15] and references therein).

The refinement technique described above equilibrates the local error over the whole mesh in several iterations and improves the finite element solution until a fixed spatial tolerance

$$\left(\sum_k \eta_k^2\right)^{1/2} \leqslant \mathrm{TOL}_x \tag{58}$$

is achieved. Coarsening takes place only after an accepted time step before starting the multilevel process. We identify regions of small errors by their η-values. We coarsen a region ω if η does not exceed a quarter of the mean square value of all η_k computed for the finest mesh.

The linear systems are solved by the BICGSTAB–algorithm preconditioned with an ILU–method.

5. Numerical simulations

The application that we study in our numerical simulations, is the cooling of a glass cube representing a typical fabrication step in glass manufacturing. We consider clean glass, which means that the treatment of scattering can be omitted. The nonopaque frequency interval (ν_0, ∞) is approximated by an eight-band model kindly provided by ITWM [23]. Since the data are originally defined by wavelength intervals $[\lambda_{i-1}, \lambda_i]$, we computed the corresponding frequency bands using the relation

$$\nu_i = \frac{c_0}{\lambda_i n_g}$$

The values used are given in Table 2. Furthermore, we set

$$k_c = 1, \qquad h_c = 0.001, \qquad T_b = 300$$

and start with a uniform temperature distribution $T_0(\mathbf{x}) = 1000$. The time integration is stopped at $t = 0.001$.

Our main interest is focused on two aspects:

- How accurate are SP_1- and SP_3-approximations?
- What is the impact of adaptivity in space and time?

To give an answer to the first question, we validate SP_N-solutions with numerical solutions to the full RHTE for $\epsilon = 1.0$ and $\epsilon = 0.1$. The full RHTE is solved by a diamond differencing discretization coupled with a discrete ordinate method which uses 60 directions [24,25]. This is for the present situation sufficient to obtain an accurate solution for the transport problem provided the spatial grid is chosen fine enough. For the second aspect, we present results obtained from applying uniform methods.

Table 2
Absorption rates of an eight frequency bands model kindly provided by ITWM [23]

Band i	ν_{i-1} [$10^{13}\mathrm{s}^{-1}$]	ν_i [$10^{13}\mathrm{s}^{-1}$]	λ_i [μm]	λ_{i-1} [μm]	κ_i [m^{-1}]
–	0	2.9334638	7.00	∞	opaque
1	2.9334638	3.4223744	6.0	7.0	7136.00
2	3.4223744	3.7334994	5.5	6.0	576.32
3	3.7334994	4.5631659	4.5	5.5	276.98
4	4.5631659	5.1335616	4.0	4.5	27.98
5	5.1335616	5.8669276	3.5	4.0	15.45
6	5.8669276	6.8447489	3.0	3.5	7.70
7	6.8447488	102.6712329	0.2	3.0	0.50
8	102.6712329	∞	0.0	0.2	0.40

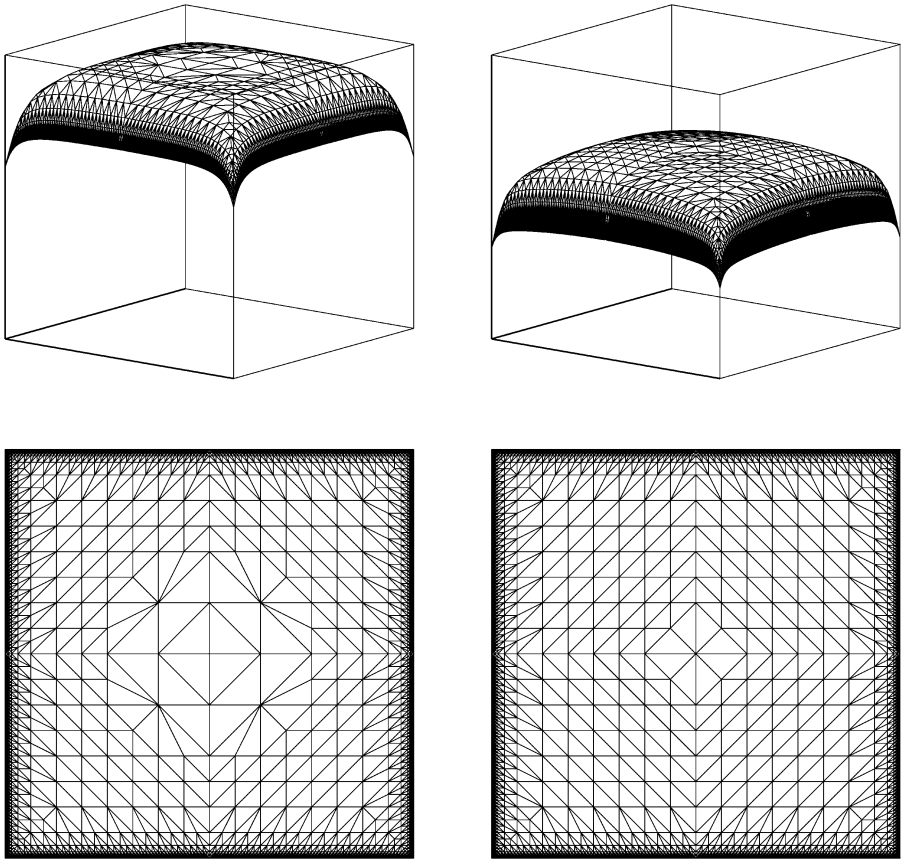

Fig. 1. Two-dimensional temperature distributions and spatial meshes on $\Omega = [0, 1]^2$ resulting from SP_3-approximations at $t_e = 0.001$ for $\epsilon = 1.0$ (left) and $\epsilon = 0.1$ (right). The temperature axis ranges from 300 to 1000. Strong refinement takes place in the boundary layer due to the large temperature gradients there.

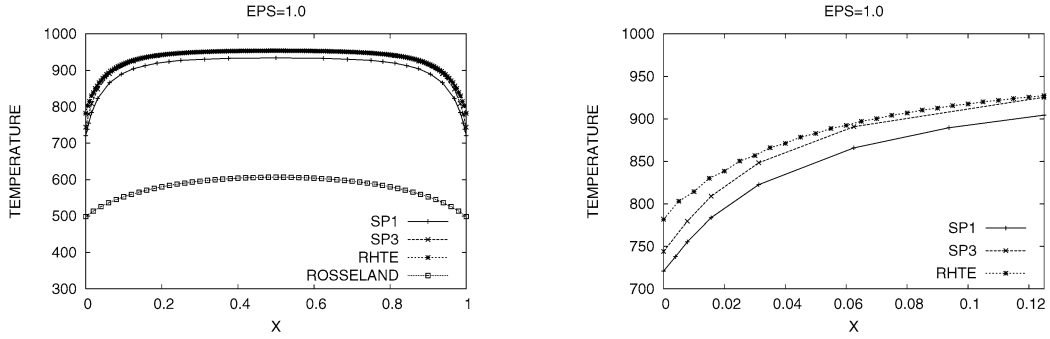

Fig. 2. Comparison of two-dimensional temperature distributions at $t_e = 0.001$ along the line $y = 0.5$ for $\epsilon = 1.0$ obtained from different radiation models. The SP_3-solution matches very well with the RHTE solution inside the glass cube. Some differences are visible in the boundary region. Both SP_N-approximations give much more accurate results than the Rosseland approximation.

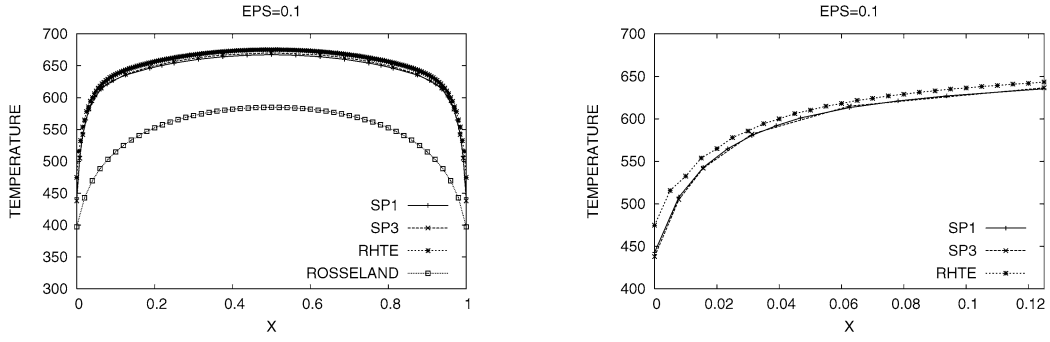

Fig. 3. Comparison of two-dimensional temperature distributions at $t_e = 0.001$ along the line $y = 0.5$ for $\epsilon = 0.1$ obtained from different radiation models. The SP_1- and SP_3-solution match very well with the RHTE solution inside the glass cube. The differences in the boundary region are acceptable. Both models give much more accurate results than the Rosseland approximation.

Two-dimensional glass cooling. We consider an infinitely long square glass block which allows us to use a two-dimensional approximation on the scaled square domain $\Omega = [0, 1]^2$.

In Fig. 1, we show temperature distributions at the final time $t_e = 0.001$ obtained for the SP_3-approximation. As expected, the strongest cooling takes place in the corners of the computational domain. The meshes automatically chosen by our adaptive approach are highly refined at the boundary caused by the steep temperature gradients there. The number of spatial points necessary to reach a relative spatial tolerance $\mathrm{TOL}_x = 0.005$ for $\epsilon = 0.1$ ranges from 16 000 at the beginning to 4000 at the end of the time interval. In this case, a stable uniform discretization of the two-dimensional RHTE requires the solution of a linear system with more than 4.8 million unknowns in each time step, whereas the dimension of the linear algebraic systems for the adaptive SP_3-approximation is not greater than 272 000.

In Figs. 2 and 3, the SP_N-solutions are compared to the full RHTE- and Rosseland approximation. As asymptotic analysis predicts, the SP_N-solutions become better for smaller ϵ. In particular, they reconstruct the temperature near the boundary much more accurately than the Rosseland approximation which is often used in engineering practice. Fig. 4 depicts the evolution of time steps using $\mathrm{TOL}_t = 0.005$. Starting with initial step sizes $\tau_1 = 1\mathrm{E}-5$ and $\tau_1 = 1\mathrm{E}-6$ for $\epsilon = 1.0$ and $\epsilon = 0.1$, respectively, the time steps rapidly increase by two orders of magnitude reflecting the ongoing diffusive smoothing in the boundary layer. The last short time steps are chosen to reach exactly the final time. Altogether 9 and 24 time steps are needed. In contrast, a uniform time discretization yielding the same accuracy, requires 100 and 1000 steps, respectively.

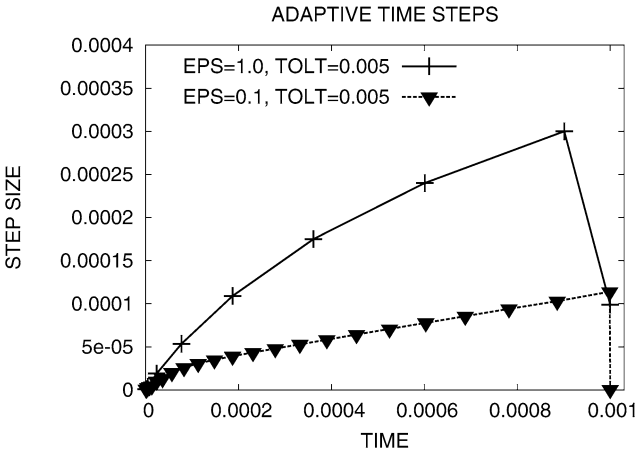

Fig. 4. Adaptive time discretization with $\mathrm{TOL}_t = 0.005$ for the two-dimensional SP_3-approximation. For both parameters, $\epsilon = 1.0$ and $\epsilon = 0.1$, the time step rapidly increases, leading to a substantial saving in computer time with respect to a constant time step procedure. The last short time steps are chosen to reach exactly the final time.

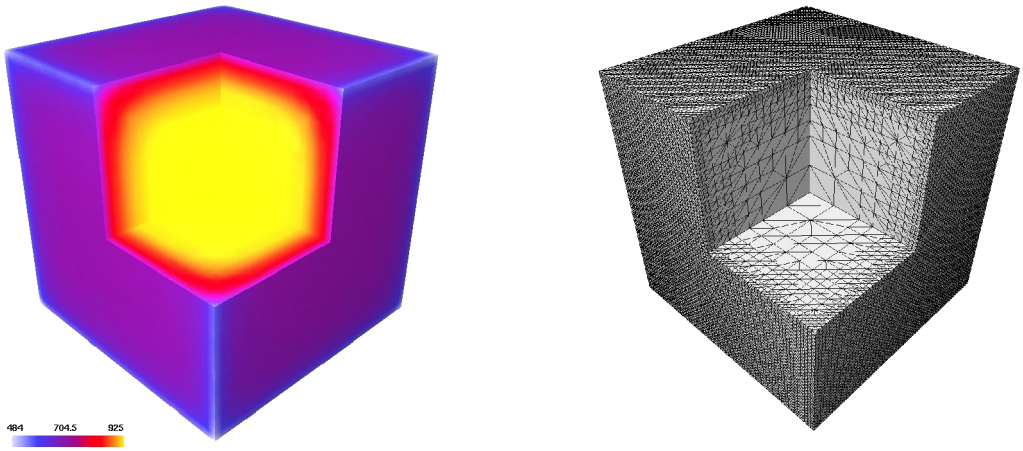

Fig. 5. Three-dimensional temperature distribution and adaptive spatial mesh on $\Omega = [0,1]^3$ resulting from the SP_3-approximation at $t_e = 0.001$ for $\epsilon = 1.0$. We removed one small cube to present details from inside the glass cube. Refinement takes place in the boundary layer due to the large temperature gradients there. The adaptive mesh consists of 82 705 grid points.

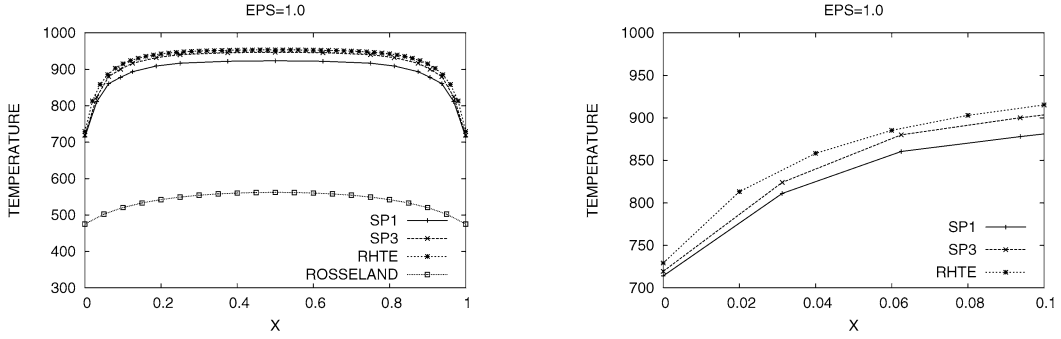

Fig. 6. Comparison of three-dimensional temperature distributions at $t_e = 0.001$ along the line $y = z = 0.5$ for $\epsilon = 1.0$ obtained from different radiation models. The SP_3-solution matches very well with the RHTE solution, whereas the Rosseland approximation gives quite poor results.

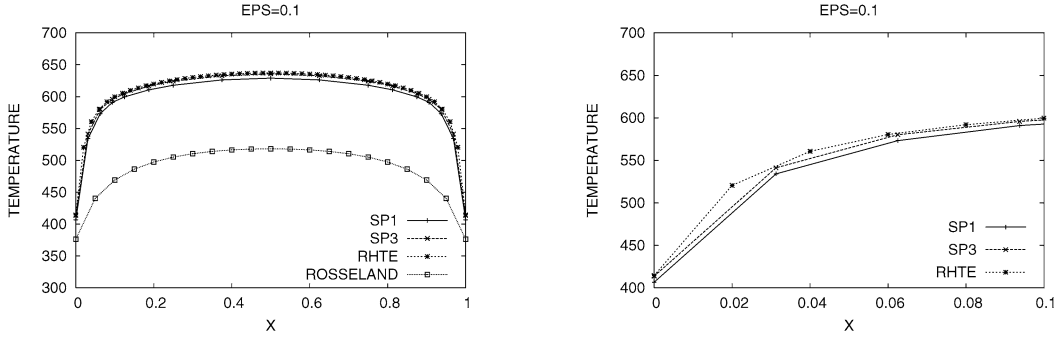

Fig. 7. Comparison of three-dimensional temperature distributions at $t_e = 0.001$ along the line $y = z = 0.5$ for $\epsilon = 0.1$ obtained from different radiation models. The SP_1- and SP_3-solution match very well with the RHTE solution and give much more accurate results than the Rosseland approximation.

Three-dimensional glass cooling. We consider a glass block which is represented by a scaled cube $\Omega = [0,1]^3$.

Fig. 5 displays the SP_3-solution for $\epsilon = 1.0$ and the adaptive three-dimensional grid chosen by our method for $\mathrm{TOL}_x = 0.01$. As already observed in the two-dimensional case, the SP_N-solutions approximate the temperature computed from the full RHTE very well. In contrast to the Rosseland approximation, they exhibit physically correct boundary layers as can be seen from Figs. 6 and 7. To accurately capture these boundary layers, the use of local refinement is essential.

The mesh shown in Fig. 5 consists of 82 705 nodes, leading to a linear system of order 1 405 985. A uniform method requires approximately 250 000 grid points to reach a comparable solution quality. The solution of the full RHTE is done on a $(100 \times 100 \times 100)$-grid, yielding a linear system with 480 million unknowns which has to be solved in each time step. The third-order ROS3P-method needs not more

than 20 adaptive time steps to integrate each of the systems in time.

Computing times. Using the method described above without adaptivity in space and time the computing times for the Rosseland approximation, the SP_1- and SP_3-model scale up like $1:7:14$. The solution of the RHTE problem by the multigrid method studied in [25] takes again approximately twice as much time as the SP_3-solution for the same accuracy. Adaptivity in space and time yield a decrease of computing times by a factor of 20 to 100. The SP_3-solution shown in Fig. 5 can be computed on a normal workstation in about 10 hours. Adaptivity reduces computing times considerably as well as enabling much more complex tasks to be solved.

6. Conclusion

We have presented a fully adaptive approach to solve simplified P_N-approximations of the radiative heat transfer equation. In order to demonstrate the potential of this method, we considered a practically relevant annealing problem arising in glass manufacturing. As already known from earlier intensive numerical investigations, the SP_N-equations are a relatively inexpensive way to improve the accuracy of classical diffusion models. Compared to the solution of full radiative heat transfer equations, the complexity and computer time are considerably reduced. Further reduction can be achieved by fully adaptive discretization methods steered by robust a posteriori error estimators.

References

[1] Y.H. Pan, W. Aung, R. Reiss, Diffusion approximations for interaction of radiation and conduction in fused silica, in: Heat Transfer Phenomena in Radiation, Combustion and Fires, volume HTD-106. National Heat Transfer Conference, 1989.

[2] M.F. Modest, Radiative Heat Transfer, second ed., McGraw-Hill, New York, 2003.

[3] R. Viskanta, E.E. Anderson, Heat transfer in semitransparent solids, Adv. Heat Transfer 11 (1975) 318–441.

[4] G. Thömmes, Radiative heat transfer equations for glass cooling problems: Analysis and numerics, PhD thesis, Technische Universität Darmstadt, 2002.

[5] S. Kuske, Modelling of radiative heat transfer in sooting flames, PhD thesis, Technical University Graz, 1999.

[6] Fluent, Fluent5 Users Guide, Fluent Inc., Lebanon NH, USA, 1999.

[7] B. van der Linden, Radiative heat transfer in glass, PhD thesis, Technische Universiteit Eindhoven, 2002.

[8] S. Chandrasekhar, Radiative Transfer, Oxford University Press, London, 1950.

[9] R. Koch, W. Krebs, S. Wittig, R. Viskanta, Discrete ordinate quadrature schemes for multidimensional radiative transfer, J. Quant. Spect. Rad. Transfer 53 (1995) 353–372.

[10] S. Rosseland, Theoretical Astrophysics. Atomic Theory and the Analysis of Stellar Atmospheres and Envelopes, Clarendon Press, Oxford, 1936.

[11] F. Lentes, N. Siedow, Three-dimensional radiative heat transfer in glass cooling processes, Glass Sci. Technol./Glasstechnische Berichte 72 (6) (1999) 188–196.

[12] E.M. Gelbard, Simplified spherical harmonics equations and their use in shielding problems, Technical Report WAPD-T-1182, Bettis Atomic Power Laboratory, 1961.

[13] E.W. Larsen, J.E. Morel, J.M. McGhee, Asymptotic derivation of the multigroup P_1 and simplified P_N equations with anisotropic scattering, Nuclear Sci. Engrg. 123 (1996) 328.

[14] E.W. Larsen, G. Thömmes, A. Klar, M. Seaïd, T. Götz, Simplified P_N approximations to the equations of radiative heat transfer and applications, J. Comput. Phys. 183 (2002) 652–675.

[15] J. Lang, Adaptive Multilevel Solution of Nonlinear Parabolic PDE Systems. Theory, Algorithm, and Applications, Lecture Notes in Comput. Sci. and Engrg., vol. 16, Springer, Berlin, 2000.

[16] J. Lang, B. Erdmann, Adaptive linearly implicit methods for heat and mass transfer problems, in: A.V. Wouver, P. Saucez, W.E. Schiesser (Eds.), Adaptive Methods of Lines, CRC Press, Boca Raton, FL, 2001, pp. 295–316.

[17] H.H. Rosenbrock, Some general implicit processes for the numerical solution of differential equations, Comput. J. 5 (1963) 329–331.

[18] J. Lang, J. Verwer, ROS3P—an accurate third-order Rosenberg solver designed for parabolic problems, BIT 41 (2001) 730–737.

[19] E. Hairer, G. Wanner, Solving Ordinary Differential Equations II, second revised ed., Springer Series in Computational Mathematics, Springer, Berlin, 1996.

[20] K. Gustafsson, M. Lundh, G. Söderlind, A PI stepsize control for the numerical solution of ordinary differential equations, BIT 28 (1988) 270–287.

[21] P. Deuflhard, P. Leinen, H. Yserentant, Concepts of an adaptive hierarchical finite element code, Impact Comput. Sci. Engrg. 1 (1989) 3–35.

[22] R. Kornhuber, F.A. Bornemann, B. Erdmann, Adaptive multilevel methods in three space dimensions, Internat. J. Numer. Methods Engrg. 36 (1993) 3187–3203.

[23] Fraunhofer-Institut für Techno- und Wirtschaftsmathematik, Kaiserslautern, Germany, http://www.itwm.de.

[24] P.N. Brown, A linear algebraic development of diffusion synthetic acceleration for three-dimensional transport equations, SIAM J. Numer. Anal. 32 (1995) 179–214.

[25] M. Seaïd, A. Klar, Generalized numerical approximations for the radiative heat transfer problems in two space dimensions, in: P. Lybaert, V. Feldheim, D. Lemonnier, N. Selçuk (Eds.), Computational Thermal Radiation in Participating Media, Elsevier, Amsterdam, 2003, pp. 419–429.